TURBULENT FLOW IN ROTATING RIB-ROUGHENED CHANNEL

Filippo Coletti, Irene Cresci and **Tony Arts**
Turbomachinery & Propulsion Department – Jacques Chauvin Laboratory
von Karman Institute for Fluid Dynamics
72 Chaussée de Waterloo, 1640 Rhode-Saint-Genèse, Belgium
coletti@vki.ac.be irene.cresci@vki.ac.be arts@vki.ac.be

ABSTRACT

The unsteady turbulent flow in a rotating channel provided with wall-mounted ribs is investigated by means of Time-Resolved Particle Image Velocimetry. Space-time series of instantaneous velocity highlight the flapping motion of the separating and reattaching shear layer, while the shedding of spanwise vortices from the ribs is visualized using the swirling strength criterion. Space-time velocity correlations provide the convection velocity, the Eulerian and the Lagrangian scales in the free shear layer behind the rib. The major effects of rotation on these flow characteristics are demonstrated: those are related to the ability of Coriolis forces of promoting/inhibiting turbulence activity depending on the mutual orientation of system angular velocity and relative mean vorticity.

INTRODUCTION

Turbulent flows in rotating frames are of considerable interest in a variety of industrial and geophysical applications, from turbomachinery to atmospheric dynamics. The system rotation leads to the appearance of Coriolis forces and centrifugal forces, but only the former play a major role in absence of density variations. In turbomachinery, one of the applications in which rotational effects are most relevant is the coolant flow in the internal cavities of rotating turbine blades. This type of flow belongs to the class of turbulent duct flows in orthogonal rotation (i.e. in which the axis of rotation is perpendicular to the stream-wise direction).

The effect of Coriolis on the shear layer stability depends on the magnitude and orientation of the background vorticity (i.e. the angular velocity of the rotating device, Ω) relative to the mean flow vorticity in the relative frame (ω): rotation is named cyclonic (anti-cyclonic) when Ω and ω are parallel (anti-parallel), in which case turbulence is damped (enhanced) by rotation. This effect was elucidated in previous experimental and numerical studies of canonical channel flows (large or infinite aspect ratios) under spanwise rotation (Johnston et al. 1972, Kristofferson and Andersson 1993). In channels of finite aspect ratio the unbalance of Coriolis forces and transverse pressure gradients near the lateral walls produce secondary flows which drive the core flow from the leading wall towards the trailing wall of the duct, an effect which was already recognized in the early experiments of Hill and Moon (1962). Studies concerned with separated flows in spanwise rotation highlighted the major impact of Coriolis forces on both mean flow and turbulence properties (Rothe and Johnston,1975; Barri and Andersson, 2010).

The measurement of accurate velocity fields in rotating frames presents severe practical difficulties, which explains the scarceness of experimental contributions in literature. In most past studies concerned with orthogonally rotating channel flows either hot wire anemometry (Nakabayashi and Kitoh, 1996) or standard Particle Image Velocimetry (Visscher et al, 2011) were used as velocimetry techniques. The former cannot identify instantaneous coherent structures, while the latter lacks sufficient temporal resolution for investigating the turbulence dynamics. This limitation is especially undesirable for separated flows, where Taylor hypothesis cannot be invoked.

Wall-mounted obstacles (ribs) are often inserted in internal cooling channels to break the boundary layer and promote secondary motions in order to enhance the heat transfer. The flow over square wall-mounted obstacles has received vast attention in the literature. When the obstacle height is significant (say of the order of the boundary layer thickness or larger) the flow is especially complicate as it becomes the combination of two already complex phenomena: the flow over the frontward-facing step (FFS) represented by the upstream side of the obstacle, and the flow over the backward-facing step (BFS) represented by its downstream side. For both such configurations the general agreement is that there are at least two dominant frequencies (Simpson, 1989): the low frequency of flapping of the separating and reattaching shear layer; and the frequency (about one order of magnitude higher) of vortex shedding from the edge of the step.

The objective of the present study is to use Time-Resolved PIV to explore the spatio-temporal structure of the turbulent flow in a rotating duct provided with transverse square ribs.

EXPERIMENTAL APPARATUS

The measurements are performed in the VKI facility for rotating channel flows (Fig. 1). It consists of a rotating disk of 2.5 m in diameter which is put in rotation around an horizontal axis by a DC motor (Fig. 1). A centrifugal fan supplies the air

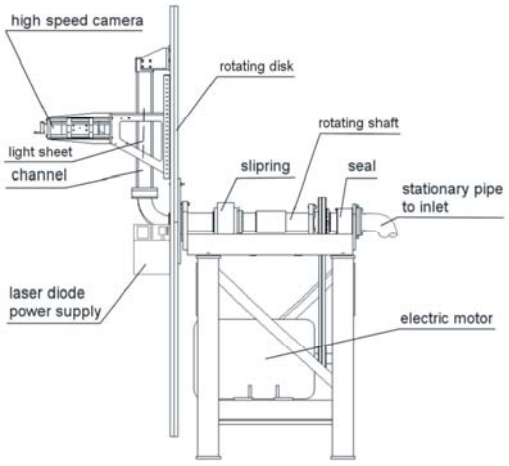

Figure 1. Lateral view of the rotating facility

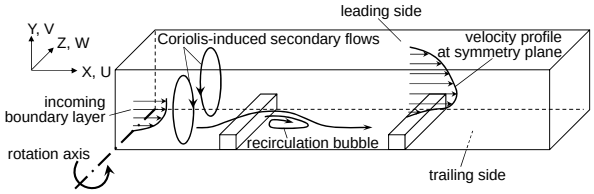

Figure 2. Schematic of the mean flow in the rotating ribbed channel under consideration

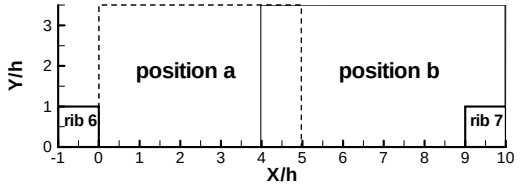

Figure 3. Location of the measurement stations and coordinate system

flow which passes through a hollow rotating shaft, turns into a 90˚ elbow and flows in the test section in the outward radial direction. As the experiment is isothermal, centrifugal forces do not induce centrifugal buoyancy. The facility is described Di Sante et al. (2008).

The test section consists of a 760 mm long rectangular channel machined out of Plexiglas. The hydraulic diameter D is 0.79 mm and the aspect ratio is 0.9. One wall parallel to the axis of rotation is provided with 8 ribs perpendicular to the flow direction; their section is 8×8 mm^2 section and their spacing is 10h, h being the rib height. The rib-spacing is sufficient for the flow to reattach after separation for all rotating and non-rotating cases; therefore the roughness can be classified as k-type (Perry et al. 1969). Further details on the test section are given in Coletti et al. (2010). The Reynolds number based on the bulk velocity U_0 is $Re=U_0D/\nu=1.5\cdot10^4$. Measurements in rotation are performed at 134 rpm, corresponding to a rotation number $Ro=\Omega D/U_0=0.38$. As the details of the flow past the obstacles are investigated, the reference length scale will be the rib height h.

Figure 2 is a schematic representation of the mean flow features expected from previous investigations (Coletti et al., 2010). U, V and W are the mean velocity components along the streamwise (X), wall-normal (Y) and spanwise (Z) direction, respectively. The sense of rotation of the secondary flow cells, which skew the velocity profile, depends on the direction of rotation. In Fig. 2 both the free shear layer behind the ribs and the redeveloping boundary layer along the ribbed wall are subject to anti-cyclonic rotation. As the facility can rotate in both senses, both cyclonic and anti-cyclonic rotations are considered in this study.

Time-resolved 2D velocity fields are measured along the streamwise/wall-normal plane at mid-span. The PIV system consists of a continuous laser diode and a CMOS high speed camera. As the measurement system rotates with the channel, the same accuracy, spatial and temporal resolution as in a non-rotating rig are achieved. Full details are given in Di Sante et al. (2008). In the present campaign two slightly overlapping windows of about 45×30 mm^2 cover the area between the 6th and 7th rib, extending in wall-normal direction up to 3.5 rib heights (Fig. 3). The magnification factor is about 13 pixel/mm, the exposure time and separation time are set at 80 μs and 300 μs respectively. The PIV processing is performed by means of a in-house cross-correlation based interrogation algorithm (Scarano and Riethmuller, 2000). The initial interrogation windows are 80×64 pixel^2. Two refinement steps and a 75% overlap lead to a final grid of 5×4 pixel^2, corresponding to an average vector spacing of 0.04h. Ensemble-averaged fields are obtained from 1000 uncorrelated realizations acquired at a sampling frequency f_S=3 Hz. Furthermore 2000 time-resolved realizations are obtained at f_S=3.3 kHz operating the PIV system in cinematographic mode (i.e. the second image of each pair is the first of the successive pair).

RESULTS

Coriolis effects on the mean flow

The system rotation results in strong modifications of the average velocity field and turbulence levels; therefore before looking into the spatio-temporal structure of the flow it is useful to summarize the main features of the mean flow. Figure 4 depicts the ensemble-averaged in-plane streamlines superimposed to the streamwise normal Reynolds stress component for the three considered cases: cyclonic rotation, non-rotating channel and anti-cyclonic rotation. The typical flow features of the flow over a rib-roughened wall are visible (Rau et al., 1998): the *vena contracta*, the large recirculation region behind the rib and the corner vortices at the bottom of each obstacle. With system rotation the secondary flows sweep the high momentum core of the flow towards the

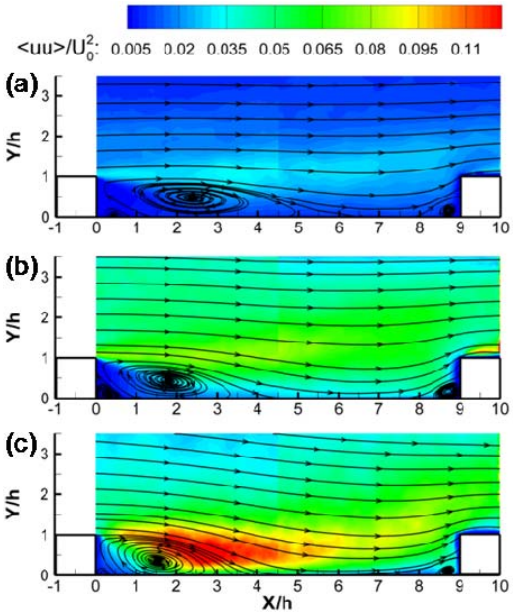

Figure 4. Mean flow streamlines and X-component of Reynolds stress tensor: cyclonic rotation (a), non-rotating channel (b) and anti-cyclonic rotation (c).

trailing wall (where rotation is anti-cyclonic); moreover Coriolis forces alter the stability of the free shear layer generated by the obstacle, resulting in an extension (reduction) of the reattachment length along the cyclonic (anti-cyclonic) side. For the present rotational regime the large recirculation, which extends up to X/h=3.75 in the non-rotating case, shrinks down to X/h=3.45 along the anti-cyclonic side, while it extends up to X/h=6 along the cyclonic side (see coordinate system in Fig. 3). The rotational effects and the underlying mechanisms were described in Coletti et al. (2010), where mean velocities and turbulence statistics were reported for the same configuration at a somewhat lower rotation number (Ro=0.3). Here it suffices to underline how the global effect of cyclonic rotation is to damp turbulent agitation both in streamwise (Fig. 4) and wall-normal direction (not shown), especially in the free shear layer behind the rib; the opposite is true for anti-cyclonic rotation. The flow is periodic in X-direction over the considered domain (Coletti et al. 2010).

Space-time series of instantaneous velocity

The time-resolved stack of acquired 2D velocity fields constitutes a three-dimensional set of data where the third dimension is time. Such volume of information allows to inspect the spatio-temporal evolution of the flow structures with great detail. For ease of representation, only 400 consecutive realizations (out of the 2000 acquired) will be visualized. In Fig. 5, 6 and 7 different time-wise sections of the data volume are presented.

Figure 5 shows the streamwise velocity just above the tip of the 7th rib (Y/h=1.1). In cyclonic rotation the flow is mostly

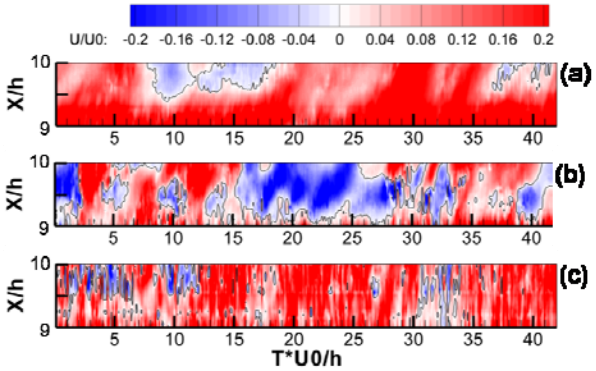

Figure 5. Space-time series of streamwise velocity above the tip of the 7th rib (Y/h=1.1): cyclonic rotation (a), non-rotating channel (b) and anti-cyclonic rotation (c)

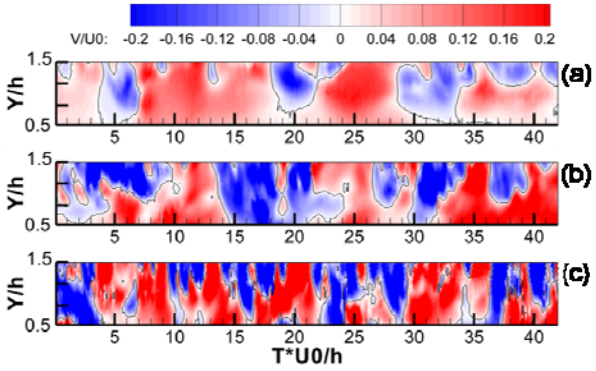

Figure 6. Space-time series of wall-normal velocity across the shear layer downstream of the 6th rib (X/h=2): cyclonic rotation (a), non-rotating channel (b) and anti-cyclonic rotation (c).

directed forward, with weak sporadic flow reversal close to the downstream edge of the obstacle. The instantaneous separation which takes place at the leading edge of the rib is too small to be properly captured already at this small wall distance. In this sense the flow past the downstream edge of the rib closely resembles the shear layer separating from a backward-facing step. In the non-rotating case an intermittent recirculation region spanning the whole rib tip is detected, in agreement with the findings of Mullin and Martin (1991). In the anti-cyclonic case the unsteady reverse flow displays a much more frenzy, irregular behavior: backflow occurs over very short periods of time and at high (although irregular) cadence.

Figure 6 shows contours of wall-normal velocity on a vertical section taken one rib height downstream of the 6th rib (X/h=1). The alternation of positive and negative velocities reflects the shear layer flapping. Clear dominant frequencies could not be identified by spectral analysis, possibly due to the complex coupling of the FFS-type with the BFS-type of flow.

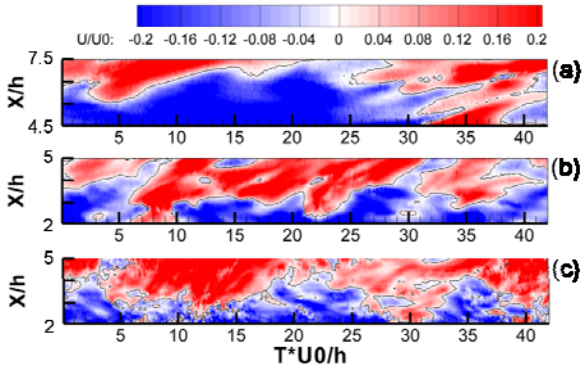

Figure 7. Space-time series of streamwise velocity around the mean reattachment point (Y/h=0.1): cyclonic rotation (a), non- rotating channel (b) and anti-cyclonic rotation (c)

However the space-time series suggest that the non-dimensional period of flapping (TU_0/h) is around 15, 12 and 7 for the cyclonic, non-rotating and anti-cyclonic case, respectively. Non-dimensional frequency of flapping in the order of fh/U_0=0.06 (i.e. a period of about 15) was found in several BFS-turbulent flow studies (e.g. Eaton and Johnston, 1980). The increase of flapping frequency with anti-cyclonic rotation must be partly due to the increase of actual incoming velocity, but also to the enhanced turbulence levels. Moreover the reduced reattachment length can affect the fluctuation of the separating shear layer; as matter of fact Heenan and Morrison (1998) argued that the flapping motion is linked to a feedback from the reattachment region.

The temporal evolution of the instantaneous reattachment point is illustrated in Fig. 7, displaying the space-time series of streamwise velocity in the vicinity of the mean reattachment (Y/h=0.1) for the three different cases. With cyclonic rotation the location of the zero-crossing point fluctuates slowly over a length of about three rib heights, whereas in the non-rotating and in the cyclonic configuration its movement is more frenzy and spans a smaller distance. In all cases the period of oscillation for reattachment is about twice the flapping period of the separating shear layer. Slow motion of the shear layer reattachment location was reported, among others, by Eaton and Johnston (1980).

Space-time evolution of spanwise vortices

The low aspect ratio of the present geometry and the Coriolis-induced secondary motions make the flow three-dimensional. However along the investigated symmetry plane the instantaneous vortices are expected to be mostly oriented spanwise. 2D PIV is then a perfectly suited tool for detecting and tracking such vortices, as long as they do not exit the measurement plane. Among the various vortex identification criteria, the value of the swirling strength λ_{ci} is applied here. λ_{ci} is the imaginary part of the locally calculated complex conjugate eigenvalues of the velocity gradient tensor. A positive value of swirling strength is a measure of fluid rotation that exclude shear vorticity (Zhou et al. 1999).

Figure 8 (left) displays a three-dimensional view of isocontours of swirling strength in the space-time domain for the non-rotating case. For this as for the rotating cases, the plotted isosurfaces correspond to 10% of the maximum λ_{ci} for each data set. Prograde vortices (i.e. vortices rotating in the same sense as the mean shear) are coloured in blue, whereas retrograde vortices in red. Unlike point-wise measurements or uncorrelated PIV realizations, the present approach provides an indication of both spatial and temporal coherence of the structures. Densely populated, long-lived vortices travels in space-time, pairing frequently to form larger structures. As expected, a majority of prograde vortices is found.

Figure 8 (right) is a top view of the spanwise vortices traveling in space-time for the three considered cases. For ease of visualization the structures are color-coded with the wall-normal distance. Vortices further from the wall are convected faster by the bulk of the flow, while those in the recirculation region (Y/h<1) remain almost at the same location over time. The velocity and the position of the fast moving structures suggest that they are generated at least at the previous obstacle (5^{th} rib), if not further upstream. The vortices travels faster in anti-cyclonic rotation, consistently with the higher velocity along the trailing wall. The three-dimensional turbulence enhanced by anti-cyclonic rotation disrupts the spanwise vortices, which show lesser coherence in both space and time with respect to the non-rotating case. The opposite holds for cyclonic rotation. Looking at the intervals between successive vortices shed just above the rib (Y/h>~1), a non-dimensional period of about TU_0/h =1.5 is estimated for the vortex shedding in the non-rotating case. This shedding frequency appear reduced (increased) in cyclonic (anti-cyclonic) rotation, due to the lower (higher) flow velocity.

Space-time velocity correlations

Correlation functions can provide useful information on the role of long-lived coherent structures: time-averaging procedures do not necessarily suppress all information on the time-dependent flow features, but can instead highlight their statistical footprints. In particular space-time correlations provide information on convection velocity of flow structures and contribute to clarify the relation between Eulerian and Lagrangian description of turbulence (Romano 1995). Space-time correlations are typically obtained from simultaneous two-point velocity measurements; time-resolved PIV gives the possibility of probing virtually any space location of the investigated plane at any time, allowing to compute space-time correlations at all locations. The space-time correlation for turbulent velocity fluctuations is:

$$R_{u_i u_j}(\vec{X}_0, \Delta\vec{X}, \Delta T) = \frac{\overline{u_i(\vec{X}_0, T_0) \cdot u_j(\vec{X}_0 + \Delta\vec{X}, T_0 + \Delta T)}}{\sqrt{\overline{u_i(\vec{X}_0, T_0)^2}} \cdot \sqrt{\overline{u_j(\vec{X}_0, T_0)^2}}} \qquad (1)$$

where u_i and u_j are the fluctuating velocity components along directions i and j, X_0 is the position vector of a fixed reference point, ΔX is the distance vector between a moving point and the reference point, T_0 is a reference time and ΔT_0 is the time

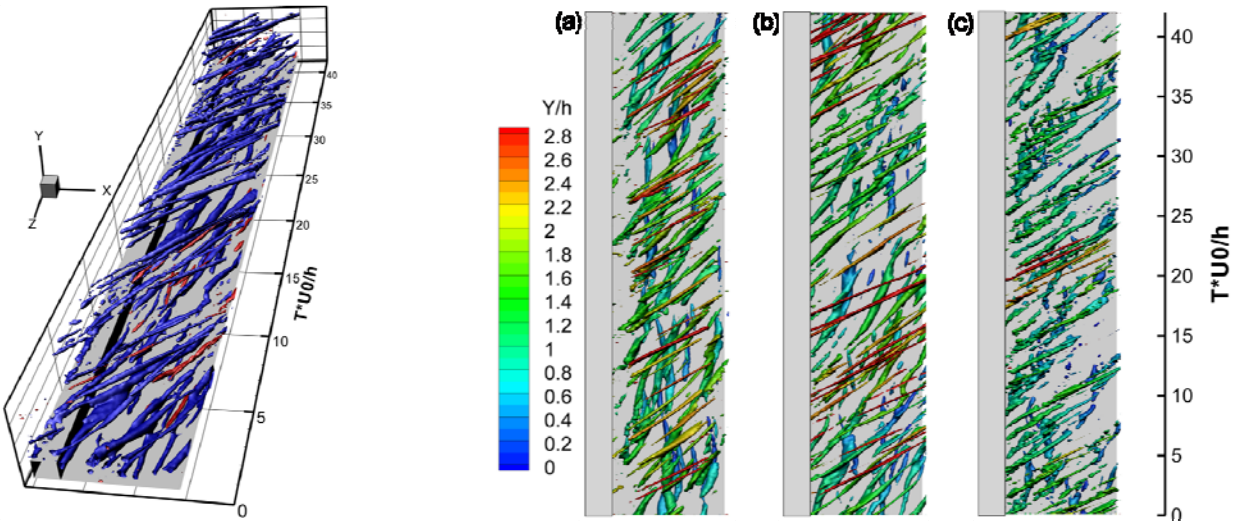

Figure 8 Spanwise vortices travelling in space-time, visualized by means of iso-contours of positive swirling strength. On the left: 3D view, with prograde vortices in blue and retrograde vortices in red. On the right: top view, color coded by wall-normal distance for cyclonic rotation (a), non- rotating channel (b) and anti-cyclonic rotation (c)

delay with respect to T_0. As the considered turbulent process is steady (in the mean sense) the correlation coefficient is independent of T_0.

Figure 9 displays isocontours of R_{uu}=0.25 for the reference point (X_0/h; Y_0/h)=(1; 1.2) in the non-rotating case. The point is chosen as it is close to a local maximum of turbulence production for the three cases. The color-code is again the wall-normal coordinate. Large-scale, quasi-periodic flow motions characterizes the free shear layer above the rib. The region of high correlation are spaced at about 15 non-dimensional time units, supporting the view of a flapping of the separated shear layer at about fh/U_0=0.06.

The contour of R_{uu}=0.5 is used here to define the integral turbulent scales, as in Volino et al. (2007): considering e.g. the streamwise coordinate, the length scale L_X^+ is taken as the distance from the self-correlation peak to the most downstream location on the R_{uu}=0.5 contour. The superscript '+' serves to indicate positive X-direction. The time scale T_X^+ is defined analogously along the time-axis. If one refers to zero-time-delay sections (ΔT=0) or zero-streamwise-spacing sections (ΔX=0) the definition above correspond to the Eulerian length scale and time scale, respectively. On the other hand the 3D iso-contour of R_{uu}=0.5 (for non-zero delay and spacing) represent the correlation coefficient in a mean flow moving frame, and therefore correspond to the Lagrangian length and time scale (Romano 1995). Figure 10 presents the R_{uu}=0.5 iso-contour for the non-rotating case. The contour is elongated along a trajectory whose slope in the ΔX-ΔT plot equals the convection velocity U_C. $L_{X,E}^+$ and $L_{X,L}^+$ (where 'E' stands for Eulerian and 'L' for Lagrangian) are indicated, along with their temporal analogues $T_{X,E}^+$ and $T_{X,L}^+$.

Figure 11 presents R_{uu}=0.5 iso-contours for t considered cases, given the same reference point specified above. Theconvection velocity U_C is about $0.6U_0$, $0.7U_0$ and$1.15U_0$ for the cyclonic, non rotating and anti-cyclonic case, respectively. These values are negligibly different from the local mean velocities. $L_{X,E}^+$ is 0.67h, 0.84h and 1.1h for the cyclonic, non-rotating and cyclonic cases. As for the Lagrangian scales, $L_{X,L}^+$ increases from the cyclonic (3.9h) to non-rotating (5.1h) and anti-cyclonic case (5.7h). The trend of $T_{X,L}^+$ is non-monotonous due to the different flow velocities for the different cases: if U_C is used as a velocity scale instead of U_0, than the trend is analogous to the one aof $L_{X,L}^+$. The increase in turbulent scales reflects the augmented turbulent activity highlighted in the mean statistics (Fig. 4).

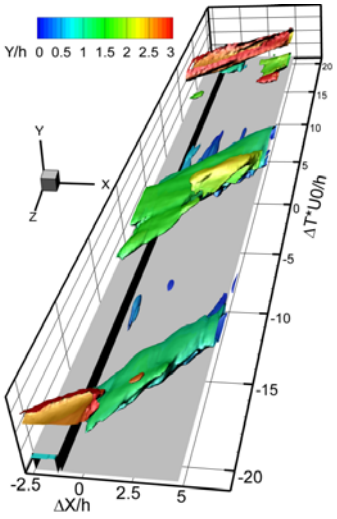

Figure 9 Iso-contours of space-time correlation R_{uu}=0.25 for the non-rotating case, color-coded by wall-normal distance. Reference point at (X_0/h; Y_0/h)=(1; 1.2)

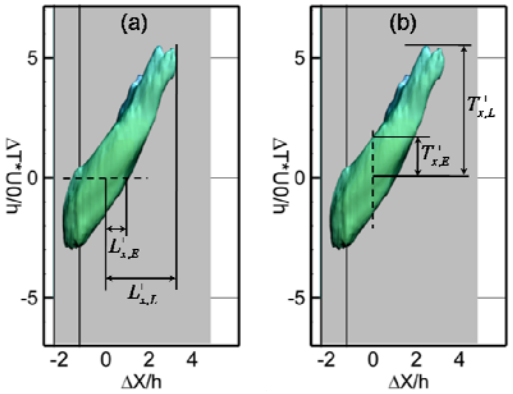

Figure 10 Definition of Eulerian and Lagrangian length scale (a) and time scales (b) with iso-contours of R_{uu}=0. Reference point at (X_0/h; Y_0/h)=(1; 1.2)

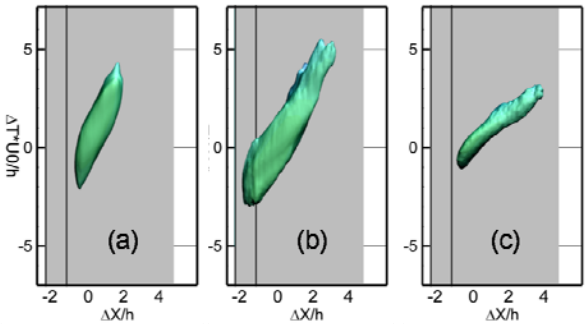

Figure 11 Iso-contours of R_{uu}=0.5 for cyclonic rotation (a), non- rotating channel (b) and anti-cyclonic rotation (c). Reference point at (X_0/h; Y_0/h)=(1; 1.2)

CONCLUSIONS

The turbulent flow in a rib-roughened rotating channel has been investigated by means of time-resolved PIV. The focus is on the area adjacent to the wall-mounted obstacles, which are square and perpendicular to the flow direction. Coriolis forces, which are known to have a major impact on the mean flow and turbulence levels, are shown to greatly modify the spatio-temporal evolution of the unsteady flow phenomena. The variation of the velocity streamlining the ribbed wall (due to Coriolis-induced secondary flows) alters the characteristic frequencies of the flow, namely the shear layer flapping and the vortex shedding from the obstacle. Anti-cyclonic rotation reduces both spatial and temporal coherence of the spanwise-vortices. The convection velocity in the free shear layer past the rib increases from cyclonic to anti-cyclonic rotation, consistently with the mean velocity trend. Lagrangian length and time scales increase with anti-cyclonic rotation, reflecting the enhancement of turbulent activity in this regime. The opposite is true for cyclonic rotation.

REFERENCES

Barri M, Andersson HI (2010) Turbulent flow over a backward-facing step. Part 1. Effects of anti-cyclonic system rotation. *J Fluid Mech* 665:382-417

Coletti F, Maurer T, Arts T, Di Sante A (2010) Flow field investigation in rotating rib-roughened channel by means of Particle Image Velocimetry, *15th Int Symp Appl Laser Tech Fluid Mech*, Lisbon, Portugal

Di Sante A, Theunissen R, Van den Braembussche RA (2008) A new facility for time resolved PIV measurements in rotating channels, *Exp Fluids* 44:179–188

Eaton JK, Johnston JP (1980) Turbulent flow reattachment: An experimental study of the flow and structure behind a backward-facing step. Stanford University, MD-39

Heenan AF, Morrison JF (1998) Passive control of backstep flow, *Exp Therm Fluid Sci* 16:122-132

Hill PG, Moon IM (1962) Effects of Coriolis on the turbulent boundary layer in rotating fluid machines. Massachusetts Institute of Technology, Report No. 69

Johnston JP, Halleen RP, Lezius DK (1972) Effects of spanwise rotation on the structure of two-dimensional fully developed turbulent channel flow. *J Fluid Mech* 56:533-557

Kristoffersen R, Andersson HI (1993) Direct simulations of low-Reynolds-number turbulent flow in a rotating channel. *J Fluid Mech* 256:163-197

Mullin T, Martin SR (1991) Intermittent phenomena in the flow over a rib roughened surface, *J Fluids Eng* 113:206-209

Nakabayashi K, Kitoh O (2005) Turbulence characteristics of two-dimensional channel flow with system rotation. *J Fluid Mech* 528:355-377

Perry AE, Schofield WH, Joubert P (1969) Rough wall turbulent boundary layers. *J Fluid Mech* 37:383-413

Rau G, Çakan M, Moeller D, Arts T (1998) The effect of periodic ribs on the local aerodynamic and heat transfer performance of a straight cooling channel. *J Turbomach* 120:368-375

Romano GP (1995) Analysis of two-point velocity measurements in near-wall flows. *Exp Fluids* 20:68-83

Rothe PH, Johnston JP (1979) Free shear layer behavior in rotating systems. *J Fluid Eng* 101:117-120

Scarano F, Riethmuller ML (2000) Advances in iterative multigrid PIV image processing. *Exp Fluids* 29:51-60

Simpson RL (1989) Turbulent Boundary Layer Separation. *Ann Rev Fluid Mech* 21:205-232

Visscher J, Andersson HI, Barri M, Didelle H, Viboudc S, Sous D, Sommeria J, (2011) A new set-up for PIV measurements in rotating turbulent duct flows, *Flow Measurement and Instrumentation* 22, 71-80

Volino RJ, Schultz MP, Flack KA (2007) Turbulence structure in rough- and smooth-wall boundary layers. *J Fluid Mech* 592:263-293

Zhou J, Adrian RJ, Balachandar S, Kendall TM (1999) Mechanism for generation of coherent packets of hairpin vortices in channel flow. *J Fluid Mech* 387:353-359